Letter

# Hidden Vibrational Bistability Revealed by Intrinsic Fluctuations of a **Carbon Nanotube**

P. Belardinelli, W. Yang, A. Bachtold,\* M. I. Dykman,\* and F. Alijani\*



Cite This: Nano Lett. 2025, 25, 8443-8449



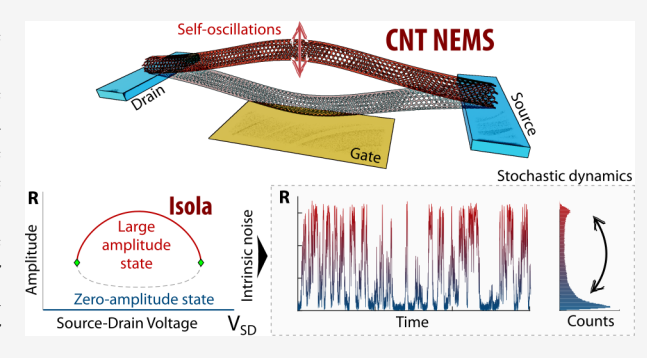
ACCESS I

III Metrics & More

Article Recommendations

Supporting Information

**ABSTRACT:** We demonstrate that a quiet state and large-amplitude self-sustained oscillations can coexist in a carbon nanotube subject to time-independent drive. A feature of the bistability is that it would be hysteresis free in the absence of noise, and the oscillatory state would not be seen. It is revealed by random switching between the stable states, which we observe in the time domain. We attribute the switching to fluctuations in the system and show that it displays Poisson statistics. We propose a minimalistic model that relates the emergence of the bistability to a nonmonotonic variation of nonlinear friction with the vibration amplitude. This new type of dynamical regime and the means to reveal it are generic and are of interest for various mesoscopic vibrational systems.



KEYWORDS: carbon nanotube, self-oscillations, hysteresis-free bistability, stochastic switching, nonlinear friction

anoelectro-mechanical systems (NEMS) provide a means for studying physics away from thermal equilibrium in a well-characterized setting. An important group of nonequilibrium phenomena originates from the interplay between nonlinearity and fluctuations in driven systems, which can modify the frequency stability, 2-6 the power spectrum, <sup>7,8</sup> lead to spectral broadening, <sup>9</sup> and thermal noise squeezing. <sup>8,10,11</sup> The interplay is most nontrivial when a nonequilibrium system is brought into a regime where it exhibits bistability. Here, fluctuations, even if weak on average, can cause interstate transitions and are ultimately responsible for the distribution of a system over the stable states. Much work on studying these effects and the emerging scaling 12,13 has been carried out on nano- and micromechanical resonators driven by an external resonant force or modulated parametrically. 7,14-23 A mechanism that leads to the onset of bistability in NEMS without periodic driving was suggested in ref<sup>24</sup> and such bistability was observed in a carbon nanotube (CNT).<sup>25</sup>

In almost all bistable mesoscopic vibrational systems, the vibrations could be brought to one of the stable states by smoothly changing a control parameter, for example, the driving force. As a result of the change, at some critical parameter value, the bifurcation point, one of the stable states would lose stability, and the system would switch to another stable state. Such behavior is usually accompanied by hysteresis: in a parameter range between bifurcation points the state of the system depends on the history of the parameter change. In all works on NEMS thus far hysteresis was used to reveal the bistability.

In this paper, we report the observation of a hysteresis-free bistability in a nanomechanical system. Such bistability means that, as the control parameter is changed back and forth, the system remains in the quiet state. The very presence of another stable state is revealed by fluctuations that cause interstate transitions. In our system, coexisting are the quiet state and the state of large-amplitude self-sustained oscillations of the lowest mode of a CNT driven by a time-independent source-drain voltage, see Figure 1. The large-amplitude oscillatory state was already identified in ref 26. It is important that the mode experiences fluctuations. We reveal that the system is actually bistable by examining the fluctuation statistics. In distinction from the more conventional scenario, the large-amplitude oscillatory state emerges as the source-drain voltage is increased, and when it emerges, it is already well separated from the quiet state in phase space. Then, as the source-drain voltage is further changed, the vibrational state is observed to lose stability. There is no hysteresis when the bifurcation parameter is moved back and forth. In terms of the bifurcation theory,<sup>27</sup> the emerging and disappearing stable states are associated with an "isola": an isolated branch of an equilibrium state of a noise-free system.

The experiment is done using clamped-clamped CNTs grown by chemical vapor deposition across two metallic contact electrodes.<sup>28</sup> The measurements are performed at

Received: December 25, 2024 Revised: April 17, 2025 Accepted: April 17, 2025 Published: April 29, 2025





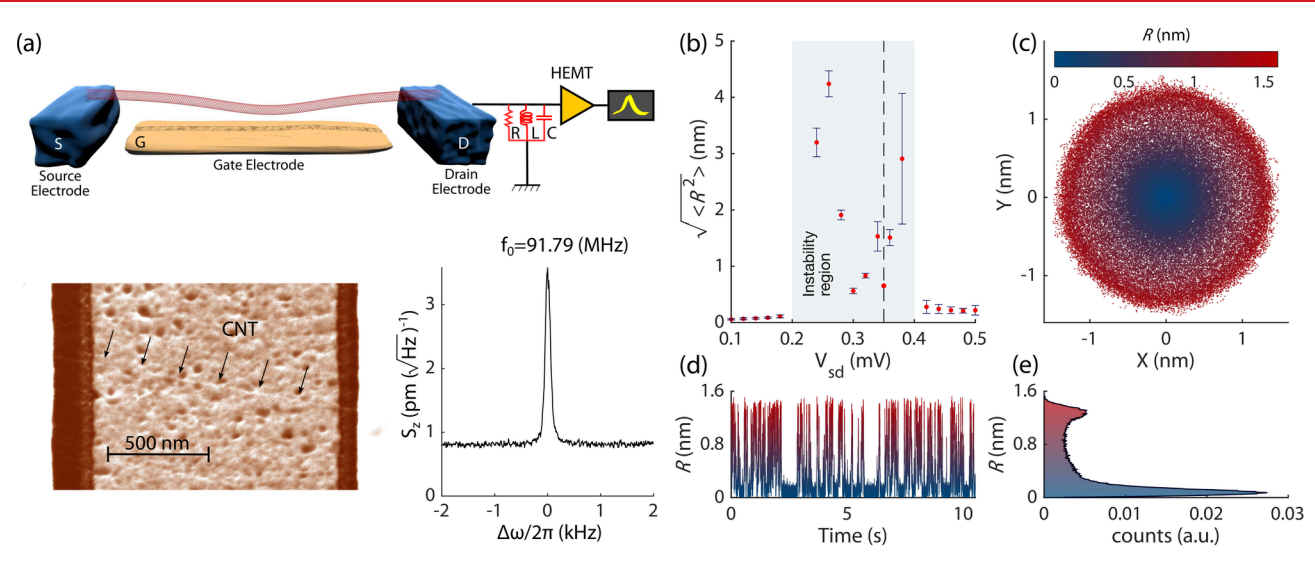


Figure 1. (a) CNT-based electromechanical oscillator and measurement schematic. The CNT has a length of  $\approx$ 1.5  $\mu$ m and a radius of  $\approx$ 1 nm (scanning electron microscope image in the bottom left panel). Voltages  $V_{\rm sd}$  and  $V_{\rm g}$  are applied to electrodes S and Gate, respectively. The drain electrode D is connected to an RLC resonator ( $f_{\rm RLC}$  = 1.27 MHz). The displacement spectral density is shown in the bottom right panel. (b) The root-mean-square nanotube displacement from the origin  $\sqrt{\langle R^2 \rangle}$  as a function of the source-drain voltage  $V_{\rm sd}$  for  $V_{\rm g}$  = -616 mV;  $\sqrt{\langle R^2 \rangle}$  is obtained from spectral noise measurements for all the data points except for  $V_{\rm sd}$  = 0.35 mV (dashed line). The latter is obtained by recording the time evolution of the displacement amplitude at the mode antinode. (c) The measured two quadratures X and Y of the motion on the (X, Y)-plane at this  $V_{\rm sd}$ . (d) Fluctuations of the amplitude  $R = \sqrt{X^2 + Y^2}$  in time for the same  $V_{\rm sd}$ . (e) Amplitude histogram, normalized with respect to the total number of observations.

cryogenic temperature (70mK) by applying a voltage bias to the source  $(V_{\rm sd})$  and to the gate electrode  $(V_{\rm g})$  which is placed beneath the CNT. The current from the drain electrode is measured by using a RLC resonant circuit and a low-temperature HEMT amplifier, see Figure 1(a). The read-out signal is obtained by measuring the current noise spectrum, which is converted to the nanotube displacement. The same calibration is used to obtain the quadratures of the motion (X,Y) from the lock-in measurements. The scaled vibration amplitude is  $R = \sqrt{X^2 + Y^2}$ .

When sweeping up the source-drain voltage  $V_{\rm sd}$  at  $V_{\rm g} = -616\,{\rm mV}$ , there occurs a sudden jump up in the displacement R for  $V_{\rm sd} \approx 0.2\,{\rm mV}$  followed by a jump down at  $V_{\rm sd} \approx 0.4\,{\rm mV}$ , see highlighted region of Figure 1(b). The change of the nanotube motion with  $V_{\rm sd}$  in Figure 1(b) does not resemble that of a vibrational system undergoing a supercritical Hopf bifurcation, whose signature is a smooth monotonic increment of the oscillation amplitude and loss of stability of the quiet state. The instability is observed over a narrow range of gate voltage  $V_{\rm g}$  but reappears periodically in  $V_{\rm g}$  with a period corresponding to adding four electrons to the nanotube. The periodicity is consistent with the SU(4) symmetry of the CNT.

In the (X,Y) space at  $V_{\rm sd}=0.35\,{\rm mV}$  we recognize a highly populated doughnut-like region centered at a nonzero mean amplitude that encircles the thermal motion about the origin of the quadrature space. This region suggests the presence of an oscillatory state, see Figure 1(c). The time trace of the motion (Figure 1(d)) and the normalized histogram of the amplitude R in Figure 1(e) further support the notion that the system has two different dynamical states. While distinct peaks in the amplitude distribution may serve as a signature of coexisting states, a double-peak pattern can also arise in various other dynamical phenomena such as intermittent chaos or bursting

oscillations.<sup>30</sup> A careful analysis is required to differentiate bistability from aperiodic dynamical behaviors.

To understand the nature of the observed dynamics, we perform statistical analysis on the time-domain data of Figure 1(d). This data set has not been presented in the earlier work. We assume that our system has two stable states, namely a zero-amplitude, i.e. a quite state, and a self-sustained oscillatory state, which has a large amplitude compared to the root-mean-square amplitude fluctuations. We investigate whether noise induces stochastic transitions between the stable states, analogous to the noise-induced interwell hopping of a damped particle in a double-well potential, see Figure 2(a), cf.; such hopping underlies stochastic resonance. The difference in our case is that here one of the stable states is a static equilibrium point, whereas the other is a state of self-sustained vibrations.

Noise-induced switching is well-defined if the switching rate is much smaller than the relaxation rate. A noise-driven system then spends most of the time fluctuating about one of its stable states. The characteristic correlation time  $t_r$  of these fluctuations is the dynamical relaxation time or the correlation time of the noise. Occasionally there occur large outbursts of noise that lead to switching between the states. The typical time between such outbursts is much larger than  $t_r$ , whereas the duration of the switching event itself is comparable to  $t_r$ . Therefore, the switching events are expected to be uncorrelated and described by the Poissonian statistics.

In order to detect interstate switching events, one would need to set a threshold, which is related to but does not coincide with the basin boundary of the two states. For a particle in a double-well potential, reaching the barrier top does not necessarily lead to switching, as the system can go back to the initially occupied well. Even in the simplest case of fluctuations induced by white noise, to find the switching rate one has to set up a threshold sufficiently far beyond the barrier

Nano Letters pubs.acs.org/NanoLett Letter

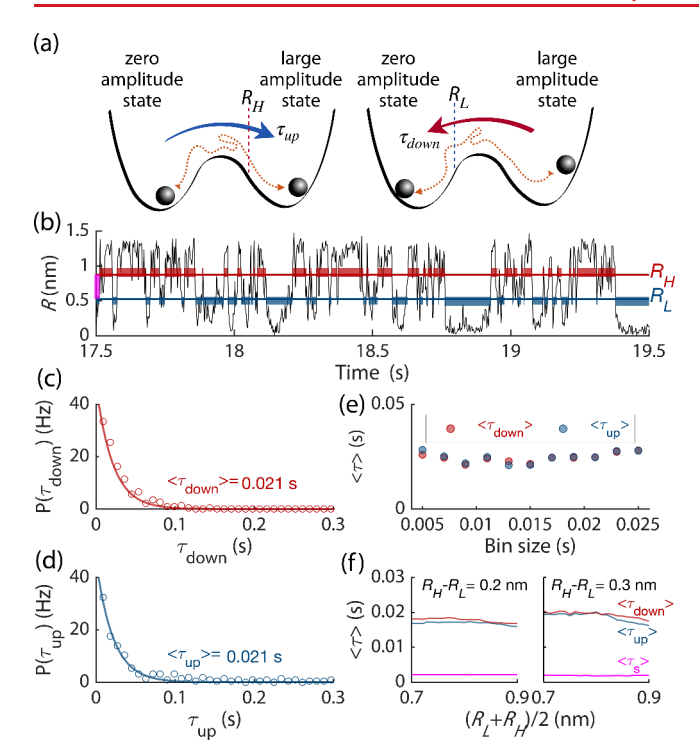


Figure 2. (a) A double-well potential, illustrating bistable dynamics using a ball-in-a-cup analogy. The minima are associated with the stable state of self-sustained vibrations and the zero-amplitude state of the CNT. Noise-induced transitions to the large-amplitude (zeroamplitude) states are considered to occur once the vibration amplitude crosses the threshold  $R_H(R_L)$ . (b) A sample of the time evolution of the vibration amplitude ( $V_{\rm sd} = 0.35 \, {\rm mV}$ ). Blue/red bars indicate the chosen switching thresholds with  $R_H - R_L = 0.35$  nm,  $(R_H + R_L)/2 = 0.7$  nm. The magenta bar indicates the region between  $R_H$  and  $R_L$ . (c, d) Dwell (residence) time distributions (bin size 9 ms) for the large-amplitude state [panel (c)] and the zero-amplitude state [panel (d)]. A Poisson distribution (eq 1) is fitted to the data. It gives averaged dwell times of  $\langle \tau_{\rm down} \rangle$  = 0.021 s and  $\langle \tau_{\rm up} \rangle$  = 0.021 s. (e) Influence of the bin size on the average dwell times in panels c and d. (f) Average dwell times for varying thresholds  $R_L$  and  $R_H$ . The average time  $\langle \tau_s \rangle$  is the time spent in between the two thresholds.

top with respect to the initially occupied state, as has been known since the classical work of Kramers.<sup>38</sup> It is clear from the above arguments that the thresholds for transitions between different states should not coincide, cf.<sup>39</sup> Hence, we introduce two amplitude thresholds,  $R_L$  and  $R_H$ , see Figure 2(a). If the system was fluctuating about R = 0 and its trajectory crossed  $R_H$ , we assume that it has switched to the large-amplitude state. On the other hand, if the system was fluctuating about the large-amplitude state and its trajectory R(t) crossed  $R_L$ , it has switched to the R = 0 state. With the above definition, the dwell (residence) times  $au_{\rm up}$  and  $au_{\rm down}$  are the times spent in the zero- and large-amplitude states, respectively, before the system switches. The time intervals  $\tau_{up}$ and  $\tau_{\text{down}}$  are shown in Figure 2(b) by the red and blue thick bars, respectively. The region between  $R_H$  and  $R_L$  contains the separatrix. The experimental data do not allow us to find it.

Figures 2(c) and 2(d) show the distribution of the dwell times  $\tau_{\rm up}$  and  $\tau_{\rm down}$ . The transitions between the states are well described by a Poisson process, and the distribution of the dwell times is close to exponential,

$$P(\tau) = \frac{1}{\langle \tau \rangle} e^{-\tau/\langle \tau \rangle} \tag{1}$$

This is the central argument in support of the coexistence of two stable states in our system. We use eq 1 to fit the experimental data and find that the dwell times are approximately the same for the chosen parameters, with  $\tau_{\rm up} \approx \tau_{\rm down} \approx 21$  ms. The fit is only mildly influenced by the bin size, see Figure 2(e). These dwell times are much larger than the relaxation time  $t_r$  of the nanotube, which can be inferred from duration of the switching events themselves: in Figure 2(b) the trajectories leading to transitions are essentially vertical. The detailed data indicates that  $t_r \sim 1-3$  ms, as illustrated in Figure 2(f) by the average time  $\langle \tau_s \rangle$  spent in between the two thresholds.

Another important argument in support of the bistability is seen from Figure 2(f). In this figure we plot the dwell times over a broad range of mean threshold values and separations. The results do not change. This demonstrates the reliability and stability of the two-threshold approach and confirms the presence of noise-induced hopping between two metastable states. The stochastic analysis conducted on an additional temporal data set, corresponding to  $V_{\rm sd} = 0.25$  mV, also aligns with these findings (see Supporting Information S1<sup>40</sup>).

The bistable dynamics observed in Figure 2 ultimately comes from the source-drain voltage  $V_{\rm sd}$ , which pumps energy into the system. The onset of self-sustained vibrations due to energy pumping is often associated with the friction coefficient becoming negative, which makes the quiet state unstable. In contrast, in our system the quiet state remains stable. This can be understood if the friction coefficient becomes negative in a certain range of sufficiently large vibration amplitude. The dependence of the friction coefficient on amplitude is called nonlinear friction. Such friction is well-known in nanomechanics. Usually it leads to a faster decay of vibrations with the increasing amplitude, that is, the coefficient of nonlinear friction is positive, although there has been also observed slowing down of the decay with the increasing amplitude.  $^{42}$ 

There are several possible causes of nonlinear friction in our system. One of them is the electron-vibrational coupling. As electrons hop between the leads and the nanoresonator, they exchange energy with the mode. This leads to decay or excitation of the vibrations, i.e., to positive or negative friction, see<sup>24,43-47</sup> and references therein. The analyses in these papers refer to the limit of strong Coulomb blockade. Negative nonlinear friction resulted from the dependence of the tunneling on the vibration amplitude.<sup>24,45</sup> This dependence should occur in our system, too, even though the Coulomb gap is moderately hard. One can picture this dependence as coming from the change of the transmission of the tunneling barrier due to the strain induced by the CNT displacement.<sup>48</sup>

In the basic model of the effect of vibrations on tunneling <sup>49</sup> the vibration-induced change of the tunneling exponent is  $C_{\rm tun}q/\lambda_{\rm tun}$ , where q is the mode coordinate and  $\lambda_{\rm tun}$  is the electron tunneling length. In the measurements presented in this work, the tunnel barriers are defined in the clamping areas at the interface between the nanotube and the metal electrodes. For tunneling onto/from a CNT, the coefficient  $C_{\rm tun}$  depends on the structure of this interface, which is not well characterized, and therefore it cannot be found quantitatively. However, the ratio  $q/\lambda_{\rm tun}$  itself is  $\gtrsim 10$  for the observed limit cycle radius and  $\lambda_{\rm tun} \sim 3-4$  Å. This suggests

Nano Letters pubs.acs.org/NanoLett Letter

that the friction that results from the modulation of the tunneling barrier can be significantly nonlinear. It can be negative in the range of  $V_{\rm sd}$  where the energy transfer to the mode exceeds the energy drain from the mode. The amplitude dependence of the friction is affected also by the polaronic effect: because of the gate voltage, electrons exert force on the mode that depends on the number of electrons on the CNT, which itself depends on the CNT displacement. This force leads to vibration decay, for strong Coulomb blockade.  $^{46}$ 

Another source of negative nonlinear friction, a retarded backaction from the circuit, is discussed in the SI Sec. S2. 40 Here, a quantitative theory requires the knowledge of the nonlinear dependence of the conductance on the vibration amplitude, which itself requires full characterization of the clamping area. However, the magnitude of this nonlinear friction force compared to the linear one is proportional to the square of the ratio of the displacement amplitude to the distance to the gate electrode and thus relatively small.

The above arguments show that the situation with nonlinear friction is no different from linear friction, which comes from several possible mechanisms. Therefore, to describe the central experimental observation, the onset and collapse of self-sustained vibrations, we use a minimalistic model. A major feature of this model is the absence of delay in the friction force, in the rotating frame. This is a consequence of the smoothness of the density of states of the electrons and thermal acoustic phonons involved in the mode decay processes, cf.<sup>1</sup>

Since the vibration frequency is much higher than all other rates and frequencies in the system, the vibrations can be described in the rotating frame using a complex vibration amplitude  $z(t) = C_z[q + i(p/m\omega_0)] \exp(i\omega_0 t)$ , where q and p are the mode coordinate and momentum, m is its effective mass,  $\omega_0$  is the eigenfrequency and  $C_z$  is a scaling parameter. In the rotating wave approximation (RWA) the equation of motion (see Sec. S3 of the Supporting Information  $^{40}$ ) reads

$$\dot{z} = -\left[\Gamma + \left(\gamma_{\rm nlf} - i\gamma_{\rm D}\right)|z|^2 + |z|^4\right]z \tag{2}$$

Here  $\Gamma$  and  $\gamma_{\rm nlf}$  are the coefficients of linear and nonlinear friction, whereas  $\gamma_D$  is the Duffing nonlinearity. The RWA applies provided  $|\dot{z}| \ll \omega_0 |z|$ . The right-hand side of eq 2 is our minimalistic model of nonlinear friction: it is an expansion in z, valid when the vibration amplitude is comparatively small, so that the decay rate and the change of the vibration frequency are  $\ll \omega_0$ . The term  $\propto |z|^4 z$  describes quintic nonlinear friction, cf. It must be taken into account where the conventional friction coefficients  $\Gamma$  and  $\gamma_{\rm nlf}$  become small. A simple microscopic model of such friction is provided in Supporting Information S4. In distinction from the conventional analysis of the onset of self-oscillations, which uses the model (2) without the quintic term, to describe the experiment we have to assume that the parameter  $\Gamma$  remains positive, and it is  $\gamma_{\rm nlf}$  that is the bifurcation parameter that changes sign.

We rewrite eq 2 in polar coordinates by setting z(t) = R(t)  $e^{i\theta(t)}$ , where R and  $\theta$  are the vibration amplitude and the "slow" part of the vibration phase. From eq 2

$$\dot{R} = -f_{\text{nlf}} R, \quad \dot{\theta} = \gamma_D R^2 \tag{3}$$

with the coefficient of nonlinear friction being

$$f_{\rm nlf} = \Gamma + \gamma_{\rm nlf} R^2 + R^4 \tag{4}$$

For  $\Gamma > 0$  the quiet state R = 0 is stable. If  $\Gamma$  becomes negative, the state R = 0 becomes unstable, and for  $\gamma_{\rm nlf} > 0$  there emerges a stable limit cycle with radius  $\propto (|\Gamma|/\gamma_{\rm nlf})^{1/2}$  (supercritical Hopf bifurcation). If  $\Gamma$  is positive but  $\gamma_{\rm nlf}$  becomes negative, there emerges an unstable limit cycle with radius  $(\Gamma/|\gamma_{\rm nlf}|)^{1/2}$  (subcritical Hopf bifurcation).

The term  $R^4$  in  $f_{\rm nlf}$  leads to the onset of a stable limit cycle for  $\gamma_{\rm nlf} < 0$  and  $\Gamma > 0$  along with an unstable one. The radii of the cycles as given by the condition  $f_{\rm nlf} = 0$  are

$$R_{\pm} = \frac{1}{\sqrt{2}} \left[ -\gamma_{\text{nlf}} \pm \sqrt{\gamma_{\text{nlf}}^2 - 4\Gamma} \right]^{1/2} \tag{5}$$

For  $-\gamma_{\rm nlf} > 2\Gamma^{1/2}$  the cycle with the radius  $R_+$  is stable, whereas the cycle with the radius  $R_-$  is unstable. At  $\gamma_{\rm nlf} = -2\Gamma^{1/2}$  the two cycles merge and annihilate one another in a saddle-node bifurcation. For smaller  $|\gamma_{\rm nlf}|/2\Gamma^{1/2}$  they disappear.

We now relate model (2) to the experiment. The values of  $\Gamma$  and  $\gamma_{\rm nlf}$  change with the control parameter  $V_{\rm sd}$ . In particular,  $\Gamma$  decreases as we approach the bistability region in Figure 1(b). The key observations are (i) a stable zero-amplitude state and a stable limit cycle coexist in a certain parameter range, (ii) the zero-amplitude state is stable not only outside, but also inside this range, and (iii) the limit cycle is excited and collapses with the varying parameters while still having a large amplitude. This scenario is qualitatively different from the standard subcritical Hopf bifurcation that is accompanied by hysteresis.

A minimalistic picture that describes the experiment is that, as the source-drain voltage  $V_{\rm sd}$  varies, there first occurs a saddle-node bifurcation at  $-\gamma_{\rm nlf}=2\Gamma^{1/2}$ . At this bifurcation there emerge the stable and unstable limit cycle with amplitudes  $R_{\pm}$ . As  $V_{\rm sd}$  varies further, these limit cycles merge together and disappear via another saddle-node bifurcation. This is illustrated in Figure 3.

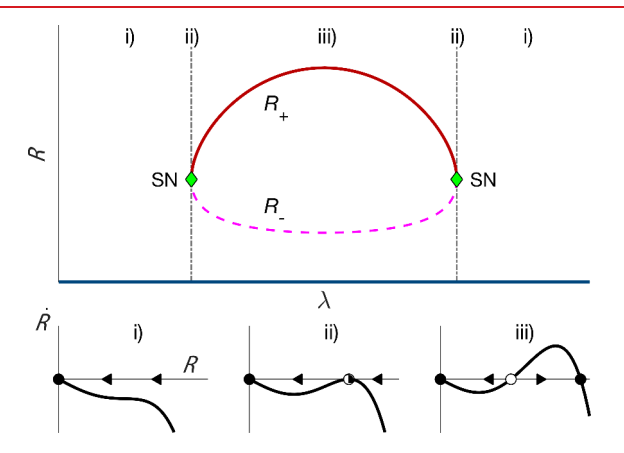


Figure 3. (Upper panel) Steady-state solutions as a function of the bifurcation parameter  $\lambda$ . In our nanomechanical resonator  $\lambda$  is a function of  $V_{\rm sd}$ . Solid/dashed lines are stable  $(R_+)$ /unstable  $(R_-)$  solution branches. The isola emerges as a result of nonmonotonic nonlinear damping. (Lower panel) Sketches of the phase portrait of the vibration radius. (i) The radial phase portrait for  $\lambda$  below and above the isola bifurcation point. The solid dot is a stable solution. (ii) The saddle-node bifurcation (SN) at a finite vibration radius, indicating the onset of an isola. (iii) Bistable region with coexisting zero and large amplitude states. The open circle is an unstable solution, which corresponds to an unstable limit cycle. The arrows in panels (i), (ii), and (iii) indicate the dynamical flow.

Nano Letters pubs.acs.org/NanoLett Letter

To link the above phenomenology to eqs 3 and 4, we should consider how the parameters of these equations depend on  $V_{\rm sd}$ . A major factor is the  $V_{\rm sd}$ -dependence of  $\gamma_{\rm nlf}$  since this parameter becomes negative and, moreover, exceeds  $2\Gamma^{1/2}$  in the absolute value. It should be noted that the linear friction coefficient  $\Gamma$  also depends on  $V_{\rm sd}$ , as reported in. <sup>26</sup> Overall,  $\gamma_{\rm nlf}$  should be nonmonotonic as a function of  $V_{\rm sd}$  to allow for both the onset and the disappearance of the bistability with the increasing  $V_{\rm sd}$ . The analysis simplifies for the gate voltage  $V_{\rm g}$  where the range of  $V_{\rm sd}$  in which the zero-amplitude state coexists with the vibrational state is narrow. In this case one can approximate

$$\gamma_{\rm nlf}(V_{\rm sd}) + 2\sqrt{\Gamma(V_{\rm sd})} = -\eta(V_B^{(1)} - V_{\rm sd})(V_{\rm sd} - V_B^{(2)})$$
 (6)

Here, the parameter  $\eta > 0$  is a scaling parameter and  $V_B^{(1,2)}$  are the bifurcational values of  $V_{\rm sd}$ . The CNT shows bistabilty in the range  $V_B^{(2)} < V_{\rm sd} < V_B^{(1)}$ .

The quadratic dependence of  $\gamma_{\rm nlf}$  and the corresponding dependence of  $R_+$  on  $V_{\rm sd}$  provide an insight into our observations, but do not fully describe the evolution of the dynamics within the instability region. The complicated dependence of  $R_+$  on  $V_{\rm sd}$  can have several causes, including defects in the CNT that lead to a nonuniform electron density, as well as the interplay of the Kondo effect and the Coulomb blockade, which depend on the bias and the gate voltage, thus modifying the tunneling and the polaronic effect and ultimately the friction force. In Figure 4 we show that the complex behavior of the vibration amplitude within the instability region can be effectively captured by considering a non-monotonic dependence of the nonlinear friction force on the

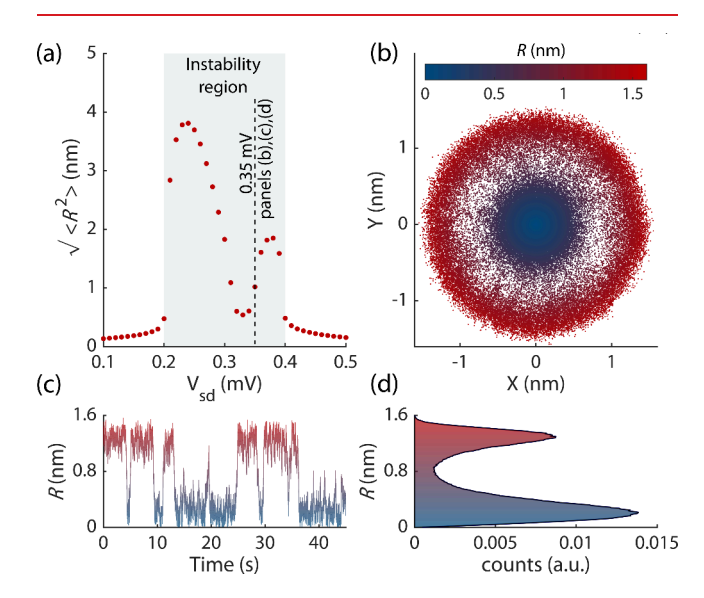


Figure 4. Numerical simulations of the fluctuation dynamics of the nanotube. (a) The standard deviation of the nanotube displacement  $\sqrt{\langle R^2 \rangle}$  as a function of the source-drain voltage  $V_{\rm sd}$ . Each point is the average of ten simulations. The stochastic dynamics is characterized for one simulation at  $V_{\rm sd}=0.35\,{\rm mV}$  (dashed line) in panels (b–d). (b) The phase space of the two quadratures of the motion (X,Y). (c) Fluctuations of the amplitude  $R=\sqrt{X^2+Y^2}$  in time. (d) The amplitude histogram of the time trace of panel (c) normalized with respect to the total number of observations. Details of the simulations of the stochastic dynamics of the nanotube are provided in Sec. S5 of the Supporting Information.

source-drain voltage. Given that the dependence of the root-mean-square vibration amplitude  $\langle R^2 \rangle^{1/2}$  on  $V_{\rm sd}$  in Figure 1(b) resembles an inverted quartic parabola, we describe the dynamics within the bistability region by a constant linear friction and a 5-parameter nonlinear friction,  $\gamma_{\rm nlf} = \sum_{n=0}^{4} (\gamma_n V_{\rm sd}^n)$ . To numerically obtain the parameters that match the experiment we positioned the saddle-node points of the isola at the boundaries of the instability region observed experimentally and constrained the amplitude of the self-oscillations to match the measured  $\sqrt{\langle R^2 \rangle}$  values.

We plot in Figure 4(a) the evolution of the amplitude variance as a function of  $V_{\rm sd}$  by simulating the stochastic dynamics of eq 2 in the quadrature space, in which each quadrature is affected by an independent random Wiener process (See Sec. S5 of the Supporting Information 40 for more details). The noise, which is white in the slow time  $\sim \Gamma^{-1}$ ,  $(|\gamma_{\rm nlf}| \langle R^2 \rangle)^{-1}$ , comes from different intrinsic sources, such as hopping of the electrons on and off the CNT and creation and annihilation of thermal phonons nonlinearly coupled to the mode. In the phase-space of the two quadratures (X,Y) the trajectories fluctuate about a circle with radius  $\langle R^2 \rangle^{1/2}$  or about the quiet state R=0, switching between them, see Figure 4(b) and (c). Respectively, the stationary probability distribution of R(t) displays two peaks, as seen in Figure 4(d).

We emphasize that the nonmonotonic dependence of the nonlinear friction parameter  $\gamma_{\rm nlf}$  on  $V_{\rm sd}$ , with  $\gamma_{\rm nlf}$  being negative in a certain range of  $V_{\rm sd}$ , is critical for the emergence of the isola and the hysteresis-free bistability. At the same time, fluctuations in the system are crucial for revealing the bistability.

Although isolas in multistable systems have attracted much attention theoretically,  $^{51-54}$  their experimental demonstrations have almost exclusively been limited to macroscale systems under periodic driving. 55-57 In mesoscopic systems, the only reported observation of isolas involves forced vibrations of a nonlinear microresonator with coupled vibrational modes.<sup>58</sup> In nanomechanis, isolas have not been observed. Here, we demonstrate the existence of an isolated vibrational state in a nanomechanical system subject to a time-independent drive. Specifically, we show that driving a carbon nanotube by a dc source-drain voltage  $V_{\rm sd}$  leads to the onset of bistability, in which a stable quiet state coexists with periodic self-sustained vibrations. We show that the bistability is nonhysteretic: varying the control parameter would not lead to switching between the branches of the stable states. We also provide a minimalistic phenomenological model that describes the effect and indicate the mechanisms that can underlie this model.

#### ASSOCIATED CONTENT

#### Supporting Information

The Supporting Information is available free of charge at https://pubs.acs.org/doi/10.1021/acs.nanolett.4c06618.

Additional analysis of statistics of stochastic switching of the carbon nanotube, discussion on friction force generated due to electrothermal backaction, theoretical description of mechanism leading to quintic nonlinear friction, and more information on numerical simulations (PDF) Nano Letters pubs.acs.org/NanoLett Lette

#### AUTHOR INFORMATION

#### **Corresponding Authors**

- A. Bachtold ICFO Institut de Ciencies Fotoniques, The Barcelona Institute of Science and Technology, 08860 Castelldefels, Barcelona, Spain; Email: Adrian.Bachtold@icfo.eu
- M. I. Dykman Department of Physics and Astronomy, Michigan State University, East Lansing, Michigan 48824, United States; Email: dykmanm@msu.edu
- F. Alijani Department of Precision and Microsystems
  Engineering, Delft University of Technology, 2628CD Delft,
  Netherlands; orcid.org/0000-0002-7439-8483;
  Email: f.alijani@tudelft.nl

#### **Authors**

- P. Belardinelli Department of Construction, Civil Engineering and Architecture, Polytechnic University of Marche, 60131 Ancona, Italy; orcid.org/0000-0003-2579-9667
- W. Yang ICFO Institut de Ciencies Fotoniques, The Barcelona Institute of Science and Technology, 08860 Castelldefels, Barcelona, Spain; orcid.org/0000-0002-3925-0352

Complete contact information is available at: https://pubs.acs.org/10.1021/acs.nanolett.4c06618

#### Notes

The authors declare no competing financial interest.

#### ACKNOWLEDGMENTS

We are grateful to Fabio Pistolesi for the discussion of the electron-phonon coupling in CNT. Financial support was provided from the European Union's research and innovation programme under ERC starting grant no. 802093, ERC consolidator grant no. 101125458, and ERC advanced grant no. 692876. M.I.D. acknowledges partial support from the U.S. Defense Advanced Research Projects Agency (Grant No. HR0011-23-2-004) and from the Gordon and Betty Moore Foundation Award GBMF12214 (doi.org/10.37807/ GBMF12214). P.B. acknowledges partial support from the European Union's NextGenerationEU programme, in the framework of PRIN 2022, project DIMIN. A.B. acknowledges MICINN Grant No. RTI2018-097953-B-I00 and PID2021-122813OB-I00, AGAUR (Grant No. 2017SGR1664), the Fondo Europeo de Desarrollo, the Spanish Ministry of Economy and Competitiveness through Quantum CCAA, TED2021-129654B-I00, EUR2022-134050, and CEX2019-000910-S [MCIN/AEI/10.13039/501100011033], MCIN with funding from European Union NextGenerationEU (PRTR-C17.I1) and Generalitat de Catalunya, CERCA, Fundacio Cellex, Fundacio Mir-Puig.

#### REFERENCES

- (1) Bachtold, A.; Moser, J.; Dykman, M. I. Mesoscopic Physics of Nanomechanical Systems. *Rev. Mod. Phys.* **2022**, *94*, 045005.
- (2) Greywall, D. S.; Yurke, B.; Busch, P. A.; Pargellis, A. N.; Willett, R. L. Evading amplifier noise in nonlinear oscillators. *Phys. Rev. Lett.* **1994**, 72, 2992–2995.
- (3) Villanueva, L. G.; Kenig, E.; Karabalin, R. B.; Matheny, M. H.; Lifshitz, R.; Cross, M. C.; Roukes, M. L. Surpassing Fundamental Limits of Oscillators Using Nonlinear Resonators. *Phys. Rev. Lett.* **2013**, *110*, 177208.

- (4) Kenig, E.; Cross, M. C.; Moehlis, J.; Wiesenfeld, K. Phase Noise of Oscillators with Unsaturated Amplifiers. *Phys. Rev. E* **2013**, 88, 062922.
- (5) Zhang, B.; Yan, Y.; Dong, X.; Dykman, M.; Chan, H. Frequency stabilization of self-sustained oscillations in a sideband-driven electromechanical resonator. *Phys. Rev. Appl.* **2024**, *22*, 034072.
- (6) Sadeghi, P.; Demir, A.; Villanueva, L. G.; Kähler, H.; Schmid, S. Frequency fluctuations in nanomechanical silicon nitride string resonators. *Phys. Rev. B* **2020**, *102*, 214106.
- (7) Stambaugh, C.; Chan, H. B. Supernarrow Spectral Peaks near a Kinetic Phase Transition in a Driven Nonlinear Micromechanical Oscillator. *Phys. Rev. Lett.* **2006**, *97*, 110602.
- (8) Huber, J. S.; Rastelli, G.; Seitner, M. J.; Kölbl, J.; Belzig, W.; Dykman, M. I.; Weig, E. M. Spectral Evidence of Squeezing of a Weakly Damped Driven Nanomechanical Mode. *Phys. Rev. X* **2020**, *10*, 021066.
- (9) Rechnitz, S.; Tabachnik, T.; Shlafman, M.; Shlafman, S.; Yaish, Y. E. Mode coupling bi-stability and spectral broadening in buckled carbon nanotube mechanical resonators. *Nat. Commun.* **2022**, *13*, 5900.
- (10) Buks, E.; Yurke, B. Dephasing Due to Intermode Coupling in Superconducting Stripline Resonators. *Phys. Rev. A* **2006**, *73*, 023815.
- (11) Yang, F.; Fu, M.; Bosnjak, B.; Blick, R. H.; Jiang, Y.; Scheer, E. Mechanically Modulated Sideband and Squeezing Effects of Membrane Resonators. *Phys. Rev. Lett.* **2021**, *127*, 184301.
- (12) Dykman, M.; Krivoglaz, M. Fluctuations in nonlinear systems near bifurcations corresponding to the appearance of new stable states. *Physica A: Statistical Mechanics and its Applications* **1980**, *104*, 480–494
- (13) Dykman, M. I. Critical exponents in metastable decay via quantum activation. *Phys. Rev. E* **2007**, *75*, 011101.
- (14) Aldridge, J. S.; Cleland, A. N. Noise-Enabled Precision Measurements of a Duffing Nanomechanical Resonator. *Phys. Rev. Lett.* **2005**, *94*, 156403.
- (15) Chan, H. B.; Stambaugh, C. Activation Barrier Scaling and Crossover for Noise-Induced Switching in Micromechanical Parametric Oscillators. *Phys. Rev. Lett.* **2007**, *99*, 060601.
- (16) Karabalin, R. B.; Lifshitz, R.; Cross, M. C.; Matheny, M. H.; Masmanidis, S. C.; Roukes, M. L. Signal Amplification by Sensitive Control of Bifurcation Topology. *Phys. Rev. Lett.* **2011**, *106*, 094102.
- (17) Venstra, W. J.; Westra, H. J. R.; van der Zant, H. S. J. Stochastic Switching of Cantilever Motion. *Nat. Commun.* **2013**, *4*, 2624.
- (18) Defoort, M.; Puller, V.; Bourgeois, O.; Pistolesi, F.; Collin, E. Scaling Laws for the Bifurcation Escape Rate in a Nanomechanical Resonator. *Phys. Rev. E* **2015**, 92, 050903.
- (19) Chowdhury, A.; Barbay, S.; Clerc, M. G.; Robert-Philip, I.; Braive, R. Phase Stochastic Resonance in a Forced Nanoelectromechanical Membrane. *Phys. Rev. Lett.* **2017**, *119*, 234101.
- (20) Dolleman, R. J.; Belardinelli, P.; Houri, S.; van der Zant, H. S. J.; Alijani, F.; Steeneken, P. G. High-Frequency Stochastic Switching of Graphene Resonators Near Room Temperature. *Nano Lett.* **2019**, 19, 1282–1288.
- (21) Steele, G. A.; Hüttel, A. K.; Witkamp, B.; Poot, M.; Meerwaldt, H. B.; Kouwenhoven, L. P.; van der Zant, H. S. J. Strong Coupling Between Single-Electron Tunneling and Nanomechanical Motion. *Science* **2009**, 325, 1103–1107.
- (22) Lassagne, B.; Tarakanov, Y.; Kinaret, J.; Garcia-Sanchez, D.; Bachtold, A. Coupling Mechanics to Charge Transport in Carbon Nanotube Mechanical Resonators. *Science* **2009**, 325, 1107–1110.
- (23) Tabanera-Bravo, J.; Vigneau, F.; Monsel, J.; Aggarwal, K.; Bresque, L.; Fedele, F.; Cerisola, F.; Briggs, G. A. D.; Anders, J.; Auffèves, A.; Parrondo, J. M. R.; Ares, N. Stability of long-sustained oscillations induced by electron tunneling. *Phys. Rev. Res.* **2024**, *6*, 013291.
- (24) Usmani, O.; Blanter, Y. M.; Nazarov, Y. V. Strong feedback and current noise in nanoelectromechanical systems. *Phys. Rev. B* **2007**, 75, 195312.

- (25) Wen, Y.; Ares, N.; Schupp, F. J.; Pei, T.; Briggs, G. A. D.; Laird, E. A. A Coherent Nanomechanical Oscillator Driven by Single-Electron Tunnelling. *Nat. Phys.* **2020**, *16*, 75–82.
- (26) Urgell, C.; Yang, W.; De Bonis, S. L.; Samanta, C.; Esplandiu, M. J.; Dong, Q.; Jin, Y.; Bachtold, A. Cooling and Self-Oscillation in a Nanotube Electromechanical Resonator. *Nat. Phys.* **2020**, *16*, 32–37. (27) Dellwo, D.; Keller, H. B.; Matkowsky, B. J.; Reiss, E. L. On the
- Birth of Isolas. SIAM J. Appl. Math. 1982, 42, 956–963.
- (28) Moser, J.; Eichler, A.; Guettinger, J.; Dykman, M. I.; Bachtold, A. Nanotube Mechanical Resonators with Quality Factors of up to 5 Million. *Nat. Nanotech* **2014**, *9*, 1007–1011.
- (29) Zakharova, A.; Vadivasova, T.; Anishchenko, V.; Koseska, A.; Kurths, J. Stochastic bifurcations and coherence-like resonance in a self-sustained bistable noisy oscillator. *Phys. Rev. E* **2010**, *81*, 011106.
- (30) Nayfeh, A. H.; Balachandran, B. Applied nonlinear dynamics: analytical, computational, and experimental methods; John Wiley & Sons, 2008.
- (31) Willick, K.; Baugh, J. Self-driven oscillation in Coulomb blockaded suspended carbon nanotubes. *Phys. Rev. Res.* **2020**, 2, 033040.
- (32) Weldon, J. A.; Alemán, B.; Sussman, A.; Gannett, W.; Zettl, A. K. Sustained Mechanical Self-Oscillations in Carbon Nanotubes. *Nano Lett.* **2010**, *10*, 1728–1733.
- (33) Feng, X. L.; White, C. J.; Hajimiri, A.; Roukes, M. L. A self-sustaining ultrahigh-frequency nanoelectromechanical oscillator. *Nat. Nanotechnol.* **2008**, *3*, 342–346.
- (34) Sekaric, L.; Zalalutdinov, M.; Turner, S. W.; Zehnder, A. T.; Parpia, J. M.; Craighead, H. G. Nanomechanical resonant structures as tunable passive modulators of light. *Appl. Phys. Lett.* **2002**, *80*, 3617–3619.
- (35) Zhang, P.; Jia, Y.; Yuan, S.; Liu, Z.; Yang, R. Tunable Stochastic State Switching in 2D MoS2 Nanomechanical Resonators with Nonlinear Mode Coupling and Internal Resonance. *Nano Lett.* **2024**, 24, 11043–11050.
- (36) Benzi, R.; Sutera, A.; Vulpiani, A. The mechanism of stochastic resonance. *Journal of Physics A: Mathematical and General* **1981**, 14, L453.
- (37) Nicolis, C. Stochastic aspects of climatic transitions—response to a periodic forcing. *Tellus* **1982**, 34, 1–9.
- (38) Kramers, H. Brownian motion in a field of force and the diffusion model of chemical reactions. *Physica* **1940**, *7*, 284–304.
- (39) Dykman, M. I.; Golubev, G. P.; Luchinsky, D. G.; Velikovich, A. L.; Tsuprikov, S. V. Fluctuational transitions and related phenomena in a passive all-optical bistable system. *Phys. Rev. A* **1991**, *44*, 2439–2449.
- (40) Supporting Information.
- (41) Keşkekler, A.; Shoshani, O.; Lee, M.; van der Zant, H. S. J.; Steeneken, P. G.; Alijani, F. Tuning Nonlinear Damping in Graphene Nanoresonators by Parametric-Direct Internal Resonance. *Nat. Commun.* **2021**, *12*, 1099.
- (42) Singh, V.; Shevchuk, O.; Blanter, Ya. M.; Steele, G. A. Negative Nonlinear Damping of a Multilayer Graphene Mechanical Resonator. *Phys. Rev. B* **2016**, *93*, 245407.
- (43) Armour, A. D.; Blencowe, M. P.; Zhang, Y. Classical dynamics of a nanomechanical resonator coupled to a single-electron transistor. *Phys. Rev. B* **2004**, *69*, 125313.
- (44) Novotný, T.; Donarini, A.; Jauho, A.-P. Quantum Shuttle in Phase Space. *Phys. Rev. Lett.* **2003**, *90*, 256801.
- (45) Fedorets, D.; Gorelik, L. Y.; Shekhter, R. I.; Jonson, M. Quantum Shuttle Phenomena in a Nanoelectromechanical Single-Electron Transistor. *Phys. Rev. Lett.* **2004**, 92, 166801.
- (46) Mozyrsky, D.; Hastings, M. B.; Martin, I. Intermittent polaron dynamics: Born-Oppenheimer approximation out of equilibrium. *Phys. Rev. B* **2006**, *73*, 035104.
- (47) Samanta, C.; De Bonis, S. L.; Møller, C. B.; Tormo-Queralt, R.; Yang, W.; Urgell, C.; Stamenic, B.; Thibeault, B.; Jin, Y.; Czaplewski, D. A.; Pistolesi, F.; Bachtold, A. Nonlinear nanomechanical resonators approaching the quantum ground state. *Nat. Phys.* **2023**, *19*, 1340–1344.

- (48) Minot, E. D.; Yaish, Y.; Sazonova, V.; Park, J.-Y.; Brink, M.; McEuen, P. L. Tuning Carbon Nanotube Band Gaps with Strain. *Phys. Rev. Lett.* **2003**, *90*, 156401.
- (49) Kagan, Y. Quantum diffusion in solids. *Journal of Low Temperature Physics* **1992**, 87, 525–569.
- (50) Strogatz, S. Nonlinear Dynamics and Chaos: With Applications to Physics, Biology, Chemistry, and Engineering; Studies in Nonlinearity; Avalon Publishing, 2014.
- (51) Habib, G.; Cirillo, G. I.; Kerschen, G. Isolated resonances and nonlinear damping. *Nonlinear Dynamics* **2018**, 93, 979–994.
- (52) Hill, T.; Neild, S.; Cammarano, A. An analytical approach for detecting isolated periodic solution branches in weakly nonlinear structures. *Journal of Sound and Vibration* **2016**, *379*, 150–165.
- (53) Cirillo, G.; Habib, G.; Kerschen, G.; Sepulchre, R. Analysis and design of nonlinear resonances via singularity theory. *Journal of Sound and Vibration* **2017**, 392, 295–306.
- (54) Mélot, A.; Denimal Goy, E.; Renson, L. Control of isolated response curves through optimization of codimension-1 singularities. *Computers & Structures* **2024**, 299, 107394.
- (55) Bureau, E.; Schilder, F.; Elmegård, M.; Santos, I. F.; Thomsen, J. J.; Starke, J. Experimental bifurcation analysis of an impact oscillator—Determining stability. *Journal of Sound and Vibration* **2014**, 333, 5464–5474.
- (56) Gatti, G.; Brennan, M. J. Inner detached frequency response curves: an experimental study. *Journal of Sound and Vibration* **2017**, 396, 246–254.
- (57) Detroux, T.; Noël, J.-P.; Virgin, L. N.; Kerschen, G. Experimental study of isolas in nonlinear systems featuring modal interactions. *PLoS One* **2018**, *13*, e0194452.
- (58) Dong, X.; Dykman, M. I.; Chan, H. B. Strong negative nonlinear friction from induced two-phonon processes in vibrational systems. *Nat. Commun.* **2018**, *9*, 3241.

# Supporting Information: Hidden vibrational bistability revealed by intrinsic fluctuations of a carbon nanotube

- P. Belardinelli,<sup>†</sup> W. Yang,<sup>‡</sup> A. Bachtold,\*,<sup>‡</sup> M.I. Dykman,\*,<sup>¶</sup> and F. Alijani\*,<sup>§</sup>
- †Department of Construction, Civil Engineering and Architecture, Polytechnic University
  of Marche, Ancona, Italy
  - ‡ICFO Institut de Ciencies Fotoniques, The Barcelona Institute of Science and Technology, 08860 Castelldefels, Barcelona, Spain
  - ¶Department of Physics and Astronomy, Michigan State University, East Lansing, MI
    48824, USA
- §Department of Precision and Microsystems Engineering, Delft University of Technology,

  Mekelweg 2, 2628CD, Delft

E-mail: Adrian.Bachtold@icfo.eu; dykmanm@msu.edu; f.alijani@tudelft.nl

# S1. Additional data on stochastic switching in the carbon nanotube

In order to demonstrate the repeatability of switching behavior within the bistable region, here we analyze an additional dataset ( $V_{\rm sd} = 0.25 \,\mathrm{mV}$  and  $V_{\rm g} = -616 \,\mathrm{mV}$ ). The findings from this supplementary data shown in Fig. S1 are consistent with our results at  $V_{\rm sd} = 0.35 \,\mathrm{mV}$  and  $V_{\rm g} = -616 \,\mathrm{mV}$  (Fig. 2 of the main manuscript). To summarize, we report: i) comparable shape of the dwell (residence) time distributions (panels c-d); ii) mild influence of the bin

size on the statistics and *iii*) dwell times unchanged over a broad range of mean threshold values and separations.

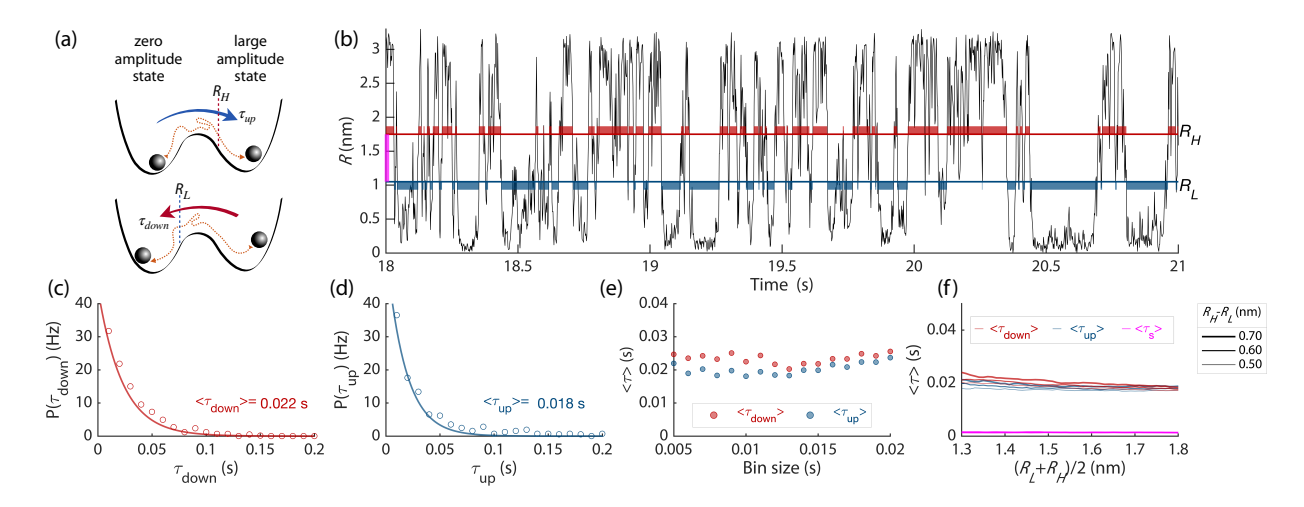


Fig. S1: (a) Sketch of a bistable potential. The minima are associated with the stable states of self-sustained vibrations and the zero-amplitude state of the CNT. Noise-induced transitions to the large-amplitude(zero-amplitude) states are considered to occur once the vibration amplitude crosses the threshold  $R_H(R_L)$ . (b) A sample of the time evolution of the vibration amplitude  $(V_{\rm sd}=0.25\,{\rm mV})$ . Blue/red bars indicate the chosen switching thresholds with  $R_H$ - $R_L$ =0.7nm,  $(R_H+R_L)/2=1.4$ nm. The magenta bar indicates the region between  $R_H$  and  $R_L$ . (c)-(d) Dwell (residence) time distributions (bin size 10 ms) for the large-amplitude state [panel (c)] and the zero-amplitude state [panel (d)]. A Poisson distribution (Eq. 1 of the main manuscript) is fitted to the data. It gives averaged dwell times of  $<\tau_{\rm down}>=0.022\,{\rm s}$  and  $<\tau_{\rm up}>=0.018\,{\rm s}$ . (e) Influence of the bin size on the average dwell times in panels d and e. (f) Average dwell times for varying thresholds  $R_L$  and  $R_H$ . The average time  $<\tau_s>$  is the time spent in between the two thresholds.

# S2. Electrothermal backaction

A possible mechanism of nonlinear friction is the electrothermal backaction due to circuit retardation. The mechanism can be viewed as follows. The nanotube displacement  $\delta z$  affects the charge on the nanotube and thus influences the nanotube conductance G. The change of the conductance  $\delta G$  can be expanded in a series in  $\delta z$ . In turn, the conductance change induces variations in the power dissipated by the current flowing through the nanotube. Through the Joule effect, the change in power  $\delta P$  leads to a temperature change  $\delta T$ . This change can be also expanded in a series in  $\delta P$ . Importantly, the temperature change modifies

the mechanical tension  $\delta T_{\rm mech}$ . To the leading order  $\delta T_{\rm mech} \propto \delta T$ . The change of the tension shifts the resonance frequency  $\delta \omega$ , thereby affecting the nanotube displacement  $\delta z$ .

This backaction mechanism is mediated by the circuit, which determines the current through the nanowire. The presence of capacitance in the circuit brings delay into the backaction, giving rise to an effective friction force. The friction force can be negative. This was shown for the linear component of the friction force in Ref. 1 The nonlinear contribution, arising from higher-order terms in the expansions mentioned above, is comparatively weaker. Roughly, the magnitude of the nonlinear friction force compared to the linear one is proportional to the square of the ratio of the displacement amplitude  $\delta z$  to the distance to the gate electrode  $z_g$ . The corresponding nonlinear friction may still be important, as it "competes" with the generally weak nonlinear friction caused by the intrinsic mechanical nonlinearity of the nanotube. But overall, because of the aforementioned smallness, we expect the nonlinear friction due to the electrothermal backaction to be weaker than the nonlinear friction arising from the backaction, which is due to the effect of the vibrations on electron tunneling.

# S3. Rotating wave approximation

This section details the derivation of Eq. 2 from the main manuscript. We assume that the mode coordinate q(t) of the nanotube is described by the single-degree-of-freedom model

$$\ddot{q} + \omega_0^2 q + \left(2\Gamma + \tilde{\gamma}_{\text{nlf}} q^2 + \Gamma_q q^4\right) \dot{q} + \tilde{\gamma}_D q^3 = 0, \tag{S1}$$

where the overdot stands for derivative with respect to time t. Furthermore,  $\omega_0$  is the radial natural frequency,  $\tilde{\Gamma}$ ,  $\tilde{\gamma}_{\rm nlf}$ ,  $\Gamma_q$  are the linear, quadratic and quintic friction coefficients, respectively. Equation (S1) includes a cubic nonlinear stiffness through the Duffing coefficient  $\tilde{\gamma}_D$ , that is associated with the geometric nonlinearity emerging due to the high mechanical compliance of the CNT. Next we transform Eq. (S1) from the fast-oscillating coordinate q(t) to slow-time variables. To that end, we utilize the complex amplitude  $\tilde{z}(t) = [q +$ 

 $i(p/m\omega_0)]\exp(i\omega_0t)$  and its complex conjugate  $\tilde{z}^*$ . Here q and p are the mode coordinate and momentum, m the effective mass,  $\omega_0$  is the eigenfrequency. The slow-dynamics in the rotating wave approximation (RWA),<sup>2</sup> is  $q(t) = \frac{1}{2} \left( \tilde{z}(t) \exp\left(-i\omega_0 t\right) + \tilde{z}^*(t) \exp\left(i\omega_0 t\right) \right)$ . We apply the method of averaging to eliminate the fast dynamics, yielding the equation for the complex amplitude  $\tilde{z}$  as follows

$$\dot{\tilde{z}} = -\Gamma \tilde{z} + \left(\frac{3i\tilde{\gamma}_D}{8\omega_0} - \frac{\tilde{\gamma}_{nlf}}{8}\right) \tilde{z}^2 \tilde{z}^* - \frac{\Gamma_q}{16} \tilde{z}^3 \tilde{z}^{*2}. \tag{S2}$$

Now, we introduce the scaling parameters  $C_z$  for the mode, that is  $z = C_z \tilde{z}$ .

The coefficients of Eq. (S2) are rescaled as  $\gamma_D = \frac{3\tilde{\gamma}_D}{8\omega_0 C_z^2}$ ,  $\gamma_{\rm nlf} = \frac{\tilde{\gamma}_{\rm nlf}}{8C_z^2}$ , and  $C_z^4 = \frac{\Gamma_q}{16}$  to obtain Eq. 2 in the main manuscript

$$\dot{z} = -\left[\Gamma + (\gamma_{\text{nlf}} - i\gamma_D)|z|^2 + |z|^4\right]z. \tag{S3}$$

## S4. Quintic nonlinear friction

A simple microscopic mechanism of quintic nonlinear friction used in the main text and described by the term  $\propto \Gamma_q$  in Eq. (S2) is the coupling to a bath described by the Hamiltonian

$$H_q = q^3 h_{\rm b} \tag{S4}$$

Here  $h_b$  is a function of the bath variables. To the lowest order in this coupling, the reaction of the bath on the vibrations can be described by the standard linear response theory,

$$\langle \delta h_{\rm b}(t) \rangle = -\int_0^\infty dt' \mathcal{X}_{\rm b}(t') q^3(t-t')$$
 (S5)

where  $\mathcal{X}_{b}(t)$  is the susceptibility of the bath.

It is seen from Eq. (S4) that the reaction (S5) leads to the backaction force from the

bath on the mode of the form  $F_q = -3q^2(t) \langle \delta h_b(t) \rangle$ . To calculate  $F_q(t)$ , one can substitute expression (S3) for x(t) into the equation for  $\langle \delta h_b(t) \rangle$ . If the Fourier transform

$$\chi_{\rm b}(\omega) = \int_0^\infty dt e^{i\omega t} \mathcal{X}_{\rm b}(t)$$

is smooth near frequency  $3\omega_0$ , one can then replace in Eq. (S5) z(t-t') and  $z^*(t-t')$  with z(t) and z(t'), respectively [cf. <sup>2,3</sup>]. One then obtaines Eq. (S2) for  $\dot{z}$  with the coefficient of quintic nonlinear friction  $\Gamma_q$  of the form

$$\Gamma_q = \frac{3}{2m\omega_0} \operatorname{Im} \chi_{\rm b}(3\omega_0) \tag{S6}$$

We note that the coupling (S4) also leads to a quintic nonlinear restoring force, which would be described by the term  $\propto |z|^4 z$  in Eq. 2 of the main manuscript. However, this term does not lead to qualitatively new results compared to the Duffing nonlinearity in the range of amplitudes we consider. The quintic nonlinear friction is needed because the coefficients of linear and standard nonlinear friction  $\Gamma$  and  $\gamma_{\rm nlf}$  are small in the absolute values in the region of coexistence of the quiet state and the state of self-sustained vibrations. We also note that quintic nonlinear friction can come from lower-order in x nonlinear coupling to the bath taken to a higher order of the perturbation theory and from a nonlinear response of the bath to such coupling.

In quantum terms, the terms in the considered coupling that are responsible for the quintic nonlinear friction have the form  $H_q = (\hbar/2m\omega_0)^{3/2}(a^3 + a^{\dagger 3})h_q$ , where a and  $a^{\dagger}$  are the ladder operators of the oscillator. They describe relaxation processes in which the oscillator goes over 3 energy levels with the energy  $\approx 3\hbar\omega_0$  transferred to the thermal bath, as indicated in the main text.

### S5. Stochastic dynamics of the nanotube

In this section, we detail out the numerical simulations of the fluctuation dynamics of the nanotube, as presented in Fig. 4 of the manuscript. Our objective is to replicate the experimental findings and qualitatively match the evolution of the slow dynamics (see Fig. 1 in the main text). To that end, we simulate the quadratures (X,Y) that correspond to the real and imaginary part of z as governed by Eq. (S3) (cf. Eq. 2 of the main manuscript). By separating the imaginary and real components, we obtain the dimensionless equations:

$$\begin{cases}
\dot{X} = -\left(\Gamma X + (\gamma_{\text{nlf}} X + \gamma_D Y) \left(X^2 + Y^2\right) + X \left(X^2 + Y^2\right)^2\right) \\
\dot{Y} = -\left(\Gamma Y + (\gamma_{\text{nlf}} Y - \gamma_D X) \left(X^2 + Y^2\right) + Y \left(X^2 + Y^2\right)^2\right)
\end{cases}$$
(S7)

As the central point of our work is that the hysteresis-free bistability is revealed through the presence of noise, we focus on the stochastic dynamics. To that end, we incorporate noise into the above equations of motion and write stochastic differential equations:

$$\begin{cases} dX = -\left(\Gamma X + (\gamma_{\text{nlf}}X + \gamma_D Y)\left(X^2 + Y^2\right) + X\left(X^2 + Y^2\right)^2\right)dt + \sigma dW_1 \\ dY = -\left(\Gamma Y + (\gamma_{\text{nlf}}Y - \gamma_D X)\left(X^2 + Y^2\right) + Y\left(X^2 + Y^2\right)^2\right)dt + \sigma dW_2 \end{cases}$$
(S8)

in which  $W_1(t)$  and  $W_2(t)$  are independent Wiener processes. These processes are constructed as normally distributed random variables with a mean of zero and a variance of dt. The asymptotic independence of these processes in the rotating frame can be traced back to the untranslated work of Bogoliubov done in 1940s, see also.<sup>2</sup>

To capture the complex variability of the amplitude observed within the instability region (Fig. 1(a) of the main text), we expand  $\gamma_{\rm nlf} = \sum_{n=0}^4 \gamma_n V_{\rm sd}^n$ . The values of  $\gamma_n$  are determined

by solving the steady state dynamics of Eq. (S3),  $\dot{z}=0$ , such that the nontrivial solution, i.e. the amplitude of the self-oscillatory state, matches the experimental datapoints. This is done by building a system of algebraic equations in the  $\gamma_n$  coefficients while imposing constraints to the vibration amplitude  $\sqrt{{\rm X}^2+{\rm Y}^2}$ . Following the experimental observation, we adjust the isolated branch such that the saddle node bifurcation points, responsible for the initialization and termination of the isola, align with the boundaries of the instability region, i.e.  $V_{\rm sd}=0.2$  and 0.4 mV. We determine the higher-order coefficients of  $\gamma_{\rm nlf}$  in Table 1. Additionally, to mimic the complex behavior of the vibration amplitude within the bistable

**Table 1:** Coefficients for the higher-order quadratic non-monotonic damping coefficient.

$\gamma_0$	$\gamma_1$	$\gamma_2$	$\gamma_3$	$\gamma_4$
2336.517	-31737.724	157406.651	-339858.316	270446.292

region, as shown in Fig. 4 of the main manuscript, we employ the coefficients  $\Gamma = 1.25$  and  $\gamma_D = 0.2$ . The system in Eq. (S8) with the set parameters is numerically integrated using the Euler-Maruyama method with  $\sigma = 0.6$ , to obtain a long-time realization (t =  $10^6$  steps with dt = 0.005) of the stochastic dynamics of the nanotube. The result of the time integration is what is shown in Fig. 4 of the main text where we study vibrational bistability revealed by noise (scaling parameter  $C_z = 1 \text{nm}^{-1} \text{s}^{-1/4}$ ).

# References

- (1) Urgell, C.; Yang, W.; De Bonis, S. L.; Samanta, C.; Esplandiu, M. J.; Dong, Q.; Jin, Y.; Bachtold, A. Cooling and self-oscillation in a nanotube electromechanical resonator.

  Nature Physics 2020, 16, 32–37.
- (2) Bachtold, A.; Moser, J.; Dykman, M. I. Mesoscopic Physics of Nanomechanical Systems. Rev. Mod. Phys. 2022, 94, 045005.

(3) Dykman, M. I.; Krivoglaz, M. A. Classical theory of nonlinear oscillators interacting with a medium. *physica status solidi (b)* **1971**, 48, 497–512.